Persistence of Logarithmic Temperature Profile in Unstably Stratified Atmospheric Boundary Layers with and Without Sand

Junning Wang[1], Jin-Han Xie[1,2(✉)], and Xiaojing Zheng[1,3]

[1] Department of Mechanics and Engineering Science at College of Engineering and State Key Laboratory for Turbulence and Complex Systems, Peking University, Beijing, China
jnwang@pku.edu.cn

[2] Joint Laboratory of Marine Hydrodynamics and Ocean Engineering, Laoshan Laboratory, Shandong 266237, People's Republic of China
jinhanxie@pku.edu.cn

[3] Center for Particle-Laden Turbulence, Lanzhou University, Lanzhou 730000, People's Republic of China
xjzheng@xidian.edu.cn

Abstract. Monin-Obukhov similarity theory (MOST) is a widely used framework in atmospheric boundary layer (ASL) research. MOST predicts that the mean potential temperature profile deviates from the logarithmic law in buoyancy-dominated turbulence. However, recent studies show that the logarithmic profile remains intact in unstably stratified atmospheric boundary layers. Using data from the Qingtu Lake Observation Array(QLOA) with Reynolds number up to O(106), we investigate the similarity functions and mean temperature profile with different stability parameters and sand-bearing conditions. By assessing the accuracy of the logarithmic profile and the MOST-based empirical expressions obtained by Hogstrom and Wilson, we discover that the logarithmic law is a better fit than the MOST expressions. The Von Kármán constant of the potential temperature profile has a power function dependences on the stability parameter. In sand-laden ASLs, it is remarkable to find that the logarithmic law still holds, and the error of the MOST expressions amplifies. The von Kármán constant of potential temperature increases in sandiness conditions. Still, a quantitative theory that describes the sand effect on the mean temperature profile remains to be studied.

Keywords: Monin-Obukhov similarity theory · unstable boundary layer · potential temperature profile

1 Introduction

The logarithmic mean velocity profile in the near-wall region of boundary-layer turbulence has been observed in laboratory and field observations and numerical

X. Zheng and S. Balachandar (Eds.): IUTAM 2023, IUTAM Bookseries 41, pp. 141–151, 2024.
https://doi.org/10.1007/978-3-031-47258-9_8

simulations [16,19,20]. Similarly, the logarithmic profile for mean temperature was also observed [15,25]. Kader [13] pointed out that the average temperature profile in wall turbulence satisfies the law of the wall. However, when buoyancy affects the flow field, the universal log law is insufficient for accurately describing the mean velocity [11,26] and temperature profiles [7,17,24,27].

Monin-Obukhov similarity theory (MOST) [21,23] is frequently used to account for buoyancy effects. MOST suggests that four parameters govern the quasi-steady turbulence structure in the Atmospheric Surface Layer (ASL): the distance z from the surface, the friction velocity u_τ (which is the square root of the magnitude of the mean kinematic surface stress), the mean temperature flux at the surface Q_0, and the buoyancy parameter g/θ_0, where θ_0 is a characteristic potential temperature. Combining the dependent variables yields dimensionless parameters. The Monin-Obukhov length is defined as $L = -\left(u_\tau\right)^3 \theta_0/\kappa g Q_0$ [22], where κ is the von Kármán constant. Thus, z/L is defined as the stability parameter. MOST implies that the mean velocity and potential temperature gradients are expressed as:

$$\frac{\kappa z}{u_\tau}\frac{\partial U}{\partial z} = \phi_m\left(\frac{z}{L}\right), \tag{1a}$$

$$-\frac{\kappa z u_\tau}{Q_0}\frac{\partial \Theta}{\partial z} = \frac{\kappa z}{\theta_\tau}\frac{\partial \Theta}{\partial z} = \phi_h\left(\frac{z}{L}\right), \tag{1b}$$

where U is the mean velocity and Θ is the mean potential temperature at the same height. ϕ_m and ϕ_h are Monin-Obukhov similarity functions. Many different forms of similarity functions have been proposed [3,4,9,14,31], and they depart from the logarithmic profiles. Particularly, Hogstrom [9] suggested:

$$\phi_h = \begin{cases} 1 + 7.8\dfrac{z}{L}, & \dfrac{z}{L} > 0, \\ \left(1 - 12\dfrac{z}{L}\right)^{-1/2}, & \dfrac{z}{L} < 0. \end{cases} \tag{2}$$

Wilson [31] proposed

$$\phi_h = \left(1 + 7.9\left|\frac{z}{L}\right|^{2/3}\right)^{-1/2} \tag{3}$$

for unstable conditions. The expression of law of the wall [28] is

$$\frac{u}{u_\tau} = \frac{1}{\kappa}\ln\frac{z}{\delta_\nu} + C, \tag{4}$$

where $\delta_\nu = \nu/u_\tau$ is the viscous length , which defines the Kármán constant.

However, recent studies find the logarithmic profile remains intact in unstably stratified atmospheric boundary layers [1,2,8,10]. It has been shown that in turbulent flows driven by both shear and buoyancy, the mean temperature profile may deviate from the traditional power law observed in Rayleigh-Bénard Convection [1,2] and natural convection [10]. Instead, a logarithmic temperature profile with varying slopes has been reported to be more prevalent than the velocity log law, and they are observed even in extremely buoyant flows [1]. These findings motivate further examination of the existence of a temperature log law in such turbulent flows. Johansson et al. [12] found that the similarity functions also depend on z_i/L, where z_i is the convective boundary layer, by performing large eddy simulations and studying field measurements. Cheng et al. [5] investigates the existence and slope of the logarithmic temperature profile in turbulent flows driven by both shear and buoyancy, such as the unstably stratified atmospheric boundary layer. Their results suggest that the buoyancy force does not modify the logarithmic nature of the mean potential temperature profile but modulates its slope instead.

Inspired by this work, we verified this conclusion under different Reynolds numbers and sediment conditions compared to theirs, examining the variables that contribute to the expression of temperature profiles. We compared the accuracy of the logarithmic profile and the MOST-based empirical expressions obtained by Hogstrom and Wilson based on the data of QLOA [18,29,30].

This paper is arranged as follows. Section 2 introduces the observation facility, data selection and pretreatment. Section 3 contains the similarity functions, mean velocity and potential temperature profiles, comparison of logarithmic profile and MOST expressions, and the slopes of the profiles vary with different abscissas. Section 4 gives the conclusions.

2 Experimental Facility and Data Details

This study utilizes data collected from the QLOA site situated on the flat and arid Qingtu Lake in western China. The observation array comprises of 21 towers, with the main tower standing at a height of 32 m and 20 smaller towers at 5 m height, all capable of measuring the three components of wind speed and dust concentration simultaneously. To measure wind speed and temperature, eleven acoustic anemometers (Campbell scientific, CSAT-3B) were mounted on the main tower between 0.9 and 30 m. The temperature measurement range is from $-40°$C to $60°$C, with a minimum resolution of $1°$C and less than $1°$C absolute error.

Due to the complexity and unpredictability of environmental conditions during field observations, specific selection and preprocessing of original data were performed to ensure accurate representation of the turbulent boundary layer at high Reynolds numbers. The pretreatment involved stratification stability judgment and classification, wind direction adjustment, and long-term trend filtering. Additionally, quality verification was conducted to ensure that the wind data were statistically stable. The non-stationary index was calculated based on the study by Foken et al. [6] to identify high-quality data with $\mathrm{IST}_u < 30\%$ and $\mathrm{IST}_\theta < 30\%$. The definition of IST_u and IST_θ is

$$\mathrm{IST}_u = \left|\left(\mathrm{CV}_{um} - \mathrm{CV}_{u1h}\right)/\mathrm{CV}_{u1h}\right| \times 100\%, \tag{5}$$

where $\mathrm{CV}_{um} = \sum_{i=1}^{12} \mathrm{CV}_{ui}/12, \mathrm{CV}_{u1}, \mathrm{CV}_{u2}, \ldots, \mathrm{CV}_{u12}$ are the streamwise velocity variances every 5 min in 1 h, and CV_{u1h} is the total streamwise velocity variance for the hour.

$$\mathrm{IST}_\theta = \left|\left(\mathrm{CV}_{\theta m} - \mathrm{CV}_{\theta 1\,h}\right)/\mathrm{CV}_{\theta 1\,h}\right| \times 100\%, \tag{6}$$

with $\mathrm{CV}_{\theta m} = \sum_{i=1}^{12} \mathrm{CV}_{\theta i}/12, \mathrm{CV}_{\theta 1}, \mathrm{CV}_{\theta 2}, \ldots, \mathrm{CV}_{\theta 12}$ are the potential temperature variances every 5 min in 1 h, and CV_{u1h} is the total potential temperature variance for the hour.

Table 1. Main parameters of the selected representative wall flow data intervals. The Re_τ of the flow is $O(10^6)$. ν is the kinematic viscosity coefficient and α is the thermal diffusion coefficient. The z/L here is calculated with the minimum experimental height 0.9m. The PM10 measured at 5m is used to reflect the amount of sediment concentration.

No	Time and date	u_τ	θ_τ	Re_τ	ν	α	z/L	PM10
		(ms^{-1})	(K)	$(\times 10^6)$	$(\times 10^{-5} m^2 s^{-1})$	$(\times 10^{-5} m^2 s^{-1})$	$(\times 10^{-3})$	$(mg \cdot m^-3)$
1	2016.3.19 12:00–13:00	0.43	−0.31	4.37	1.47	2.05	−20.6	–
2	2017.3.27 17:00–18:00	0.46	−0.15	4.67	1.47	2.04	−9.4	0.023
3	2016.3.28 10:00–11:00	0.27	−0.23	2.81	1.46	2.03	−21.3	0.075
4	2016.3.28 17:00–18:00	0.16	−0.34	1.64	1.48	2.06	−90.6	0.060
5	2016.5.14 8:00–9:00	0.48	−0.12	4.96	1.45	2.02	−3.3	0.432
6	2017.3.27 10:00–11:00	0.34	−0.21	3.54	1.44	2.01	−12.9	0.050

High-quality data with $\mathrm{IST}_u < 30\%, \mathrm{IST}_\theta < 30\%$ are selected in the work. Unstable stratified data is mainly studied. The used data were measured from 2015 to 2017 and can be classified into two types: sand-laden flow data observed during sandstorm weather and clean air data measured in clean air with little sand.

As shown in Table 1, several intervals are selected to analyze the data. No.1 is a clean air data and N0.2–N0.6 are data measured in sandstorm. $\theta_\tau = Q_0/u_\tau$ is the friction temperature. Negative z/L and θ_τ corresponds to an unstable situation. The kinetic viscosity coefficient and thermal diffusion coefficient of them have little difference. The key distinction is the stability parameter and sediment concentration. The measured data of 0.9m and 10.24m is applied in the calculation of z/L and PM10 separately.

From Fig. 1, the kinetic flux and potential temperature flux are relatively steady with elevation change, which indicates the defined characteristic parameters u_τ and θ_τ can be applicable to each height for both sets of data. No significant change is observed due to the presence of sediment.

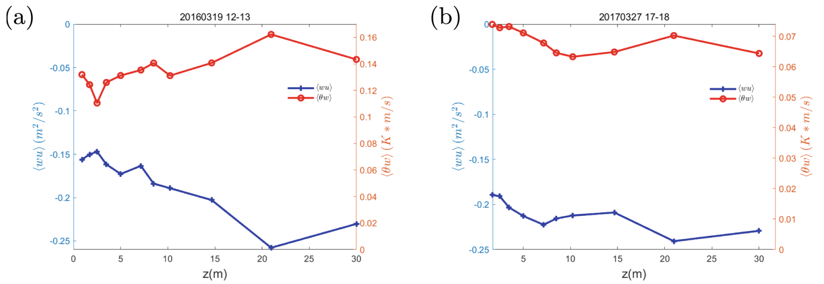

Fig. 1. $\langle wu \rangle$ and $\langle w\theta \rangle$ of clean air and sand-laden flow. Q_0 equals $\langle w\theta \rangle$ on the surface. (a) The kinetic surface flux and potential temperature flux of different heights in clean air with u_τ and θ_τ on the top right corner The blue line is $\langle wu \rangle$ while the red line is $\langle w\theta \rangle$. (b) The flux in a sand-laden flow.

3 Results

3.1 Similarity Functions

Figure 2 shows the similarity functions of the measured data and verifies the expressions of Businger [3] and Hogstrom [9]. Businger suggests the approximate expression is:

$$\phi_h = \begin{cases} 0.74 + 4.7\dfrac{z}{L}, & \dfrac{z}{L} > 0, \\ 0.74\left(1 - 9\dfrac{z}{L}\right)^{-1/2}. & \dfrac{z}{L} < 0. \end{cases} \tag{7}$$

This work focus on the unstable condition, so only the negative z/L data is plotted. In Fig. 2, measured value of ϕ_h at several heights and different time intervals are plotted. ϕ_h of different heights at the same time is close to each other. Hogstrom's formula exhibits better performance than Businger's, but discrepancies with our experimental data still exists. The predicted values are widely underestimated but the general trend is consistent with the empirical formula. The similarity functions for the sand-laden and clean air cases are essentially equivalent.

3.2 The Potential Temperature Profile

Similar to Eq. (4), the potential temperature profile expression is:

$$\frac{\Theta - \Theta_0}{\theta_\tau} = \frac{1}{\kappa_\theta} \ln \frac{z}{z_r}, \tag{8}$$

where Θ is the mean potential temperature, Θ_0 is the mean potential temperature at the lowest height, κ_θ is the potential temperature Kármán constant, and z_r is the reference height.

Figure 3 is the potential temperature profile. The horizontal axis is $z^+ = z/\delta_\nu = zu_\tau/\nu$ and the vertical axis is $\Theta^+ = (\Theta - \Theta_0)/\theta_\tau$. The predicted profile

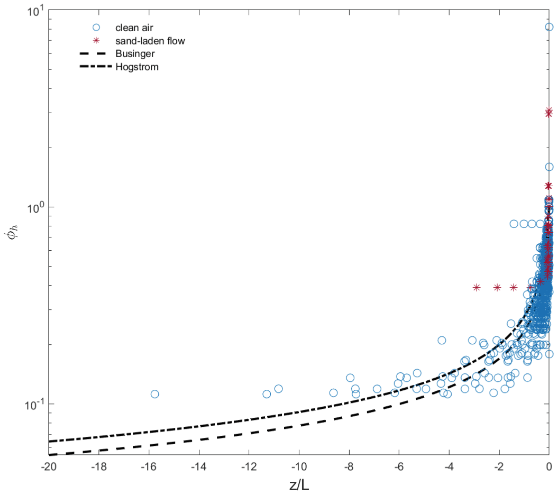

Fig. 2. Similarity function ϕ_h of clean air and sand-laden flow. The circles are the clean air data and the asterisks are the sand-laden data. The dotted line is Businger's (1971) expression and the dot dash line is Hogstrom's(1988) expression. The figure has a logarithmic ordinate.

of Hogstrom and Wilson deviates more from the measured data than the clean air situation.

In unstable conditions, the mean temperature grows with height. It can be seen from the left figure that both the three estimates of the profile under the clear wind flow are in good agreement with the actual measured data. Under the sand-laden flow, the measured data has a larger fluctuation and the two empirical expressions deviate more from the logarithmic profile. The potential temperature profiles in sand-laden flow have larger fluctuation than clean air, but they still satisfy the logarithmic profile in general.

3.3 The Root-Mean-Square Error (RMSE) Comparison of Log Law and MOST-Based Empirical Equations

To assess the accuracy of the logarithmic law equation and the MOST-based empirical equations, we computed the root mean square error (RMSE) between the measured temperature (Θ_i) and the estimated temperature ($\hat{\Theta}_i$). The RMSE is defined as:

$$\sigma_{l,H,W} = \sqrt{\frac{1}{n}\sum_{i=1}^{n}(\Theta_i - \hat{\Theta}_i)^2}, \tag{9}$$

where n represents the total number of data points. The subscripts l, H, and W correspond to the logarithmic law expression, Hogstrom's expression, and Wilson's expression, respectively. A smaller value of σ indicates a lower error, indicating a better fit between the estimated and measured temperatures.

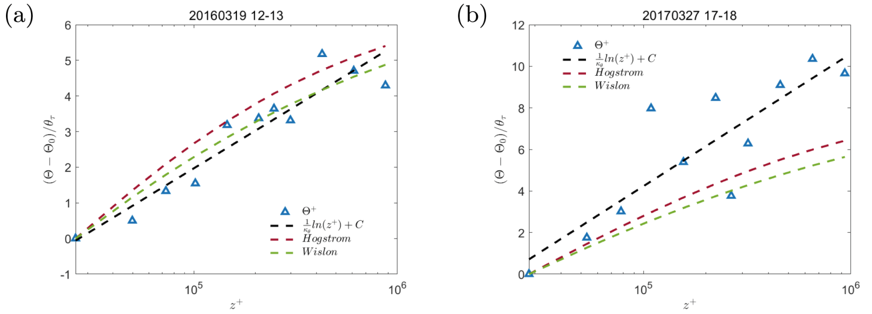

Fig. 3. The potential temperature profiles of clean air and sand-laden flow. The titles represent the time of data measurement. The triangular scatters are the measured potential temperature. The black dashed line is the log law line. The red and green lines are the MOST-based empirical results. Subfigure (a) is the clean air while (b) is the sand-laden flow.

From Fig. 4, the logarithmic coordinate plot, it can be seen that error in unstable conditions is unexpectedly smaller than in near-neutral conditions. σ has a straight line tendency in the logarithmic graph and the log law equation always has the minimum error.

The presence of sand particles does not significantly affect the error, as there is no significant difference of RSME between the sand-laden flow and clean air scenarios. The error of two empirical formulas is consistently higher than the log law equation.

The conclusion remains in the sand-laden flow. The log-law expression has the least error in all cases. Strong unstable conditions have smaller errors than weak unstable conditions. The PM10 concentration's influence is not remarkable (Fig. 5).

3.4 Slope of the Potential Temperature Profile

This section shows the dependents of κ_θ on different parameters.

We discover that the logarithmic profile remains in even strong unstable conditions when the buoyancy term plays an important role in turbulence. Different stability conditions mainly impact the slope of the mean temperature profile. The slope of the profile equals $\theta_\tau/\kappa_\theta$. The Kármán constants are power functions of $-\delta_\tau/L$, $-u_\tau^2/gL$, $-(\nu^2/g)^{1/3}/L$ and $-(\alpha^2/g)^{1/3}/L$ from Fig. 6. The abscissa employed distinct dimensionless characteristic lengths from the boundary layer flow.

Based on the fitting results of Fig. 6, we have:

$$\kappa_\theta = C_1\left(-\frac{\nu}{u_\tau L}\right)^{0.251} \approx C_1\left(-\frac{\nu}{u_\tau L}\right)^{4/15}, \tag{10a}$$

$$\kappa_\theta = C_2\left(-\frac{u_\tau^2}{gL}\right)^{0.642} \approx C_2\left(-\frac{u_\tau^2}{gL}\right)^{2/3}, \tag{10b}$$

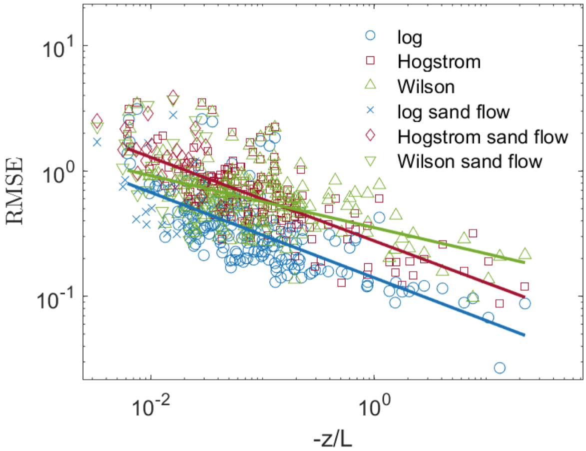

Fig. 4. RMSE of different expressions. Different color and different marker styles represent different equations' RMSE. The straight lines denotes the trends.

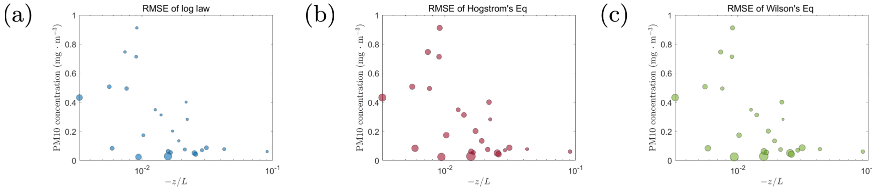

Fig. 5. RMSE of sand-laden flow. The color and size represent the value of RMSE. A larger size indicates that RMSE is larger.

$$\kappa_\theta = C_3 \left(-\frac{\nu^{2/3}}{g^{1/3}L}\right)^{0.347} \approx C_3 \left(-\frac{\nu^{2/3}}{g^{1/3}L}\right)^{1/3}, \tag{10c}$$

$$\kappa_\theta = C_4 \left(-\frac{\alpha^{2/3}}{g^{1/3}L}\right)^{0.338} \approx C_4 \left(-\frac{\alpha^{2/3}}{g^{1/3}L}\right)^{1/3}, \tag{10d}$$

where $C_{1,2,3,4}$ are constants. As Table 1 shows, ν and α vary slightly at different time intervals and can be approximated as constants.

Equation (10b) and Eq. (10c) can be rewritten as:

$$u_\tau = g^{1/2}(-L)^{1/2} \left(\frac{\kappa_\theta}{C_2}\right)^{3/4}, \quad \nu = g^{1/2}(-L)^{3/2} \left(\frac{\kappa_\theta}{C_3}\right)^{9/2}. \tag{11}$$

Substituting them in Eq.(10a), we get:

$$C_1 = \frac{C_3^{6/5}}{C_2^{1/5}}, \tag{12}$$

which shows that the scalings are consistent. The Kármán constant in the sand-laden situation has little difference with clean air conditions. A larger PM10 give rise to a larger bias from the trend line. The sand-laden data has same slope but larger κ_θ in the logarithmic plots than clean air data. A rough estimate gives that κ_θ in sand-laden data is 20–40% higher compared to clean air. However, the number of sandstorm data point is quite small. To verify the conclusion, more data from different experiment condition should be used for verification in the future.

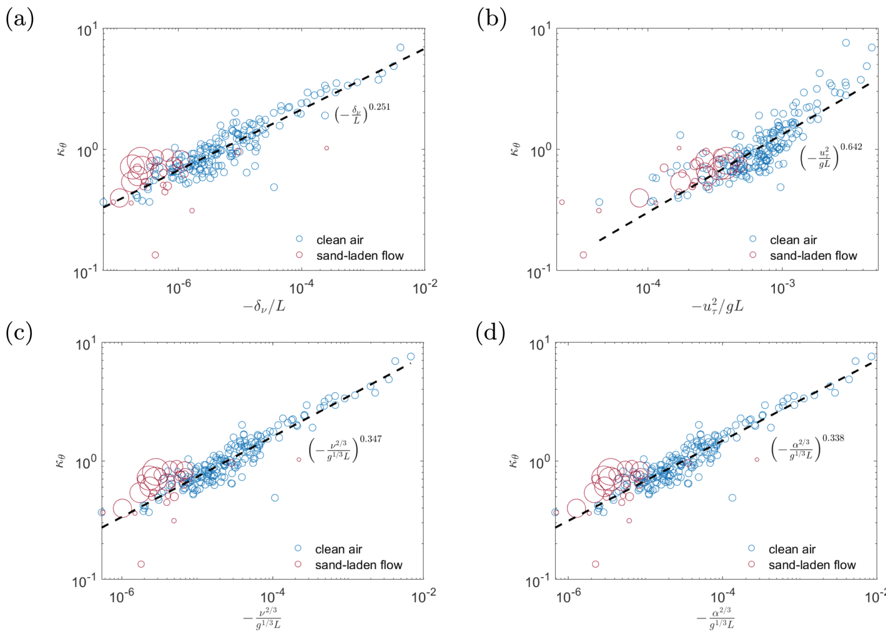

Fig. 6. The velocity and potential temperature Kármán constant of clean air and sand-laden flow. The clean air data markers are blue and the sand-laden data markers are red. Larger red circles represent larger PM10 concentrations. The dotted lines are the trend lines calculated by logarithmic polynomial fitting. Different horizontal coordinates are used in the subfigures.

4 Conclusion and Discussion

We verified the logarithmic law remains valid even in the presence of unstably stratified atmospheric conditions by investigating QLQA data with and without sand. By studying the similarity functions, potential temperature profile, root-mean-square error and slope of the profiles, we find that when buoyancy effects become significant, the empirical equations derived from the Monin-Obukhov similarity theory do not exhibit superior performance compared to the logarithmic law. We focus on the impact of stability parameters on the Kármán constant of the potential temperature profile, κ_θ. A power expression of κ_θ about

u_τ and Obukhov length L is found. $\kappa_\theta = C_1\left(-\frac{\nu}{u_\tau L}\right)^{4/15}$, $\kappa_\theta = C_2\left(-\frac{u_\tau^2}{gL}\right)^{2/3}$ and $\kappa_\theta = C_3\left(-\frac{\nu^{2/3}}{g^{1/3}L}\right)^{1/3}$. Flows containing sand have approximately $20-40\%$ higher κ_θ values compared to sand-free flows.

Due to the limited data, we do only provide qualitative impact of sand on the mean temperature profile, and the quantitative effect should be studied in the future. Also, we need theoretical explanations to the scalings for the Kármán constant of the potential temperature profile.

References

1. Ahlers, G., et al.: Logarithmic temperature profiles in turbulent Rayleigh-Bénard convection. Phys. Rev. Lett. **109**(11), 114501 (2012)
2. Ahlers, G., Bodenschatz, E., He, X.: Logarithmic temperature profiles of turbulent Rayleigh–Bénard convection in the classical and ultimate state for a prandtl number of 0.8. J. Fluid Mech. **758**, 436–467 (2014)
3. Businger, J.A., Wyngaard, J.C., Izumi, Y., Bradley, E.F.: Flux-profile relationships in the atmospheric surface layer. J. Atmos. Sci. **28**(2), 181–189 (1971)
4. Carl, D.M., Tarbell, T.C., Panofsky, H.A.: Profiles of wind and temperature from towers over homogeneous terrain. J. Atmos. Sci. **30**(5), 788–794 (1973)
5. Cheng, Yu., Li, Q., Li, D., Gentine, P.: Logarithmic profile of temperature in sheared and unstably stratified atmospheric boundary layers. Phys. Rev. Fluids **6**(3), 034606 (2021)
6. Foken, T., Göockede, M., Mauder, M., Mahrt, L., Amiro, B., Munger, W.: Post-field data quality control. In: Lee, X., Massman, W., Law, B. (eds.) Handbook of Micrometeorology. Atmospheric and Oceanographic Sciences Library, vol. 29, pp. 181–208. Springer, Dordrecht (2004). https://doi.org/10.1007/1-4020-2265-4_9
7. Garai, A., Kleissl, J., Sarkar, S.: Flow and heat transfer in convectively unstable turbulent channel flow with solid-wall heat conduction. J. Fluid Mech. **757**, 57–81 (2014)
8. Grossmann, S., Lohse, D.: Logarithmic temperature profiles in the ultimate regime of thermal convection. Phys. Fluids **24**(12), 125103 (2012)
9. Högström, U.L.F.: Non-dimensional wind and temperature profiles in the atmospheric surface layer: a re-evaluation. Top. Micrometeorol. A Festschrift Arch Dyer, pp. 55–78 (1988)
10. Hölling, M., Herwig, H.: Asymptotic analysis of the near-wall region of turbulent natural convection flows. J. Fluid Mech. **541**, 383–397 (2005)
11. Iida, O., Kasagi, N.: Direct numerical simulation of unstably stratified turbulent channel flow (1997)
12. Johansson, C., Smedman, A.-S., Högström, U., Brasseur, J.G., Khanna, S.: Critical test of the validity of Monin–Obukhov similarity during convective conditions. J. Atmos. Sci. **58**(12), 1549–1566 (2001)
13. Kader, B.A.: Temperature and concentration profiles in fully turbulent boundary layers. Int. J. Heat Mass Transf. **24**(9), 1541–1544 (1981)
14. Kader, B.A., Yaglom, A.M.: Mean fields and fluctuation moments in unstably stratified turbulent boundary layers. J. Fluid Mech. **212**, 637–662 (1990)
15. Kawamura, H., Abe, H., Matsuo, Y.: DNS of turbulent heat transfer in channel flow with respect to Reynolds and Prandtl number effects. Int. J. Heat Fluid Flow **20**(3), 196–207 (1999)

16. Lee, M., Moser, R.D.: Direct numerical simulation of turbulent channel flow up to. J. Fluid Mech. **774**, 395–415 (2015)
17. Li, D., Luo, K., Fan, J.: Buoyancy effects in an unstably stratified turbulent boundary layer flow. Phys. Fluids **29**(1), 015104 (2017)
18. Liu, H., Wang, G., Zheng, X.: Amplitude modulation between multi-scale turbulent motions in high-Reynolds-number atmospheric surface layers. J. Fluid Mech. **861**, 585–607 (2019)
19. Marusic, I., Monty, J.P., Hultmark, M., Smits, A.J.: On the logarithmic region in wall turbulence. J. Fluid Mech. **716**, R3 (2013)
20. McNaughton, K.G.: Turbulence structure of the unstable atmospheric surface layer and transition to the outer layer. Bound.-Layer Meteorol. **112**, 199–221 (2004)
21. Monin, A.S., Obukhov, A.K.: Basic laws of turbulent mixing in the surface layer of the atmosphere. Contrib. Geophys. Inst. Acad. Sci. USSR **151**(163), e187 (1954)
22. Obukhov, A.: Trudy inta teoret. Geofiz. Akad. Nauk. SSSR **1**, 95 (1946)
23. Obukhov, A.: Turbulence in thermally inhomogeneous atmosphere. Trudy Inst. Teor. Geofiz. Akad. Nauk SSSR **1**, 95–115 (1946)
24. Pirozzoli, S., Bernardini, M., Verzicco, R., Orlandi, P.: Mixed convection in turbulent channels with unstable stratification. J. Fluid Mech. **821**, 482–516 (2017)
25. Redjem-Saad, L., Ould-Rouiss, M., Lauriat, G.: Direct numerical simulation of turbulent heat transfer in pipe flows: effect of Prandtl number. Int. J. Heat Fluid Flow **28**(5), 847–861 (2007)
26. Scagliarini, A., Einarsson, H., Gylfason, Á., Toschi, F.: Law of the wall in an unstably stratified turbulent channel flow. J. Fluid Mech. **781**, R5 (2015)
27. Sid, S., Dubief, Y., Terrapon, V.: Direct numerical simulation of mixed convection in turbulent channel flow: on the Reynolds number dependency of momentum and heat transfer under unstable stratification. In: 8th International Conference on Computational Heat and Mass Transfer (2015)
28. Von Kármán, T.: Mechanical similitude and turbulence. Number 611. National Advisory Committee for Aeronautics (1931)
29. Wang, G., Zheng, X.: Very large scale motions in the atmospheric surface layer: a field investigation. J. Fluid Mech. **802**, 464–489 (2016)
30. Wang, G., Zheng, X., Tao, J.: Very large scale motions and pm10 concentration in a high-re boundary layer. Phys. Fluids **29**(6), 061701 (2017)
31. Wilson, D.K.: An alternative function for the wind and temperature gradients in unstable surface layers. Boundary-Layer Meteorol. **99**, 151–158 (2001)